Explaining the x-ray nonlinear susceptibility of diamond and silicon near absorption edges

B Barbiellini, Yves Joly, Kenji Tamasaku

Explaining the x-ray nonlinear susceptibility of diamond and silicon near absorption edges

B. Barbiellini,[1] Y. Joly,[2,3] and Kenji Tamasaku[4]
[1]*Department of Physics, Northeastern University, Boston, Massachusetts 02115, USA*
[2]*Université Grenoble Alpes, Institut NEEL, F-38042 Grenoble, France*
[3]*CNRS, Institut NEEL, F-38042 Grenoble, France*
[4]*RIKEN SPring-8 Center, 1-1-1 Kouto, Sayo-cho, Sayo-gun, Hyogo 679-5148, Japan*
(Received 14 May 2015; published 12 October 2015)

We report the observation and the theoretical explanation of the parametric down-conversion nonlinear susceptibility at the K-absorption edge of diamond and at the L_{23}-absorption edge of a silicon crystal. Using arguments similar to those invoked to successfully predict resonant inelastic x-ray spectra, we derive an expression for the renormalization term of the nonlinear susceptibility at the x-ray edges, which can be evaluated by using first-principles calculations of the atomic scattering factor f_1. Our model is shown to reproduce the observed enhancement of the parametric down-conversion at the diamond K and the Si L_{23} edges rather than the suppression previously claimed.

DOI: 10.1103/PhysRevB.92.155119 PACS number(s): 78.70.Ck, 71.15.Mb, 71.15.Qe, 78.40.Fy

I. INTRODUCTION

The advent of x-ray free-electron lasers (XFELs) [1–3] has enabled advances in the study of x-ray nonlinear processes [4], which are similar to nonlinear optics investigations and applications, that have followed the invention of the laser in 1960. Few x-ray nonlinear processes have already been observed with conventional x-ray sources. In particular, x-ray parametric down-conversion (PDC) is an intriguing second-order nonlinear process where an x-ray pump photon of energy E_p decays spontaneously into two photons, the idler and the signal with energies E_i and E_s, respectively. PDC was first discussed theoretically by Freund and Levine [5] and was then observed experimentally by Eisenberger and McCall [6,7] in 1971. The first observations of the PDC into the extreme ultraviolet (EUV) were reported by Danino and Freund [8] about a decade later. This effect has recently been used to visualize the local optical response to EUV radiation with an atom scale resolution [9]. Further improvement of PDC has recently been proposed by Shwartz and collaborators [10].

As illustrated in Fig. 1, x-ray PDC takes place as nonlinear diffraction in crystals with energy and momentum conservation laws given by

$$\begin{aligned} E_p &= E_i + E_s, \\ \mathbf{k}_p + \mathbf{Q} &= \mathbf{k}_i + \mathbf{k}_s, \end{aligned} \tag{1}$$

where $\mathbf{k}_s$, $\mathbf{k}_i$, and $\mathbf{k}_p$ are the wave vectors of the signal, idler, and pump photons, respectively, whereas $\mathbf{Q}$ is a crystal reciprocal lattice vector. The momentum conservation is also called the phase-matching condition, and rocking the crystal means scanning the phase-matching condition. Surprisingly, Tamasaku and Ishikawa observed asymmetric rocking curves, having not only a peak, but also a distinct dip [11]. If there were no interactions between the PDC and the Compton scattering, the rocking curve should be a Lorentzian peak on a smooth Compton background. Instead, the rocking curve is not simple but reveals an interference with the background Compton process. The resulting line shape is similar to the one considered by Fano [12], Vittorini-Oregas and Bianconi [13]. From the analysis of the Fano line shape, Tamasaku *et al.* [14] extracted the PDC nonlinear susceptibility $\chi^{(2)}$. These authors noticed that a sharp peak of the nonlinear susceptibility reveals a strong resonant enhancement at the K-absorption edge of diamond. This observation contradicts previous models claiming that the core resonance suppresses the nonlinear process rather than enhances it [15].

We present here a renormalization factor η that captures the behavior of the nonlinear susceptibility $\chi^{(2)}$ at the K-absorption edge of diamond and at the L_{23}-absorption edge of Si. A similar term has recently been used to explain the enhancement of the cross section observed in the resonant inelastic x-ray scattering (RIXS) [16]. The factor η is derived by using the renormalization-group method that describes the variation in the effective coupling constant under changes of scales [17–19] and the method of dispersion relations applied to the atomic scattering factor.

The remainder of this article is organized as follows. After the introductory remarks contained in Sec. I, Sec. II introduces the model and reviews the derivation of the renormalization factor η. In Sec. III, we present the methods for the calculations of the atomic scattering factor f_1 used to obtain η and for the x-ray PDC experiments. The theoretical results are presented and compared with the experimental results in Sec. IV. Important predictions of our model and the conclusions are reported in Sec. V.

II. THEORETICAL MODEL

As explained by Freund and Levine [5], the origin of the PDC nonlinearity is the Doppler shift where the induced valence charge at the idler frequency scatters x rays at a different frequency. An effective theory for this process is therefore equivalent to an inelastic x-ray scattering by valence electrons oscillating in the idler field. In the proximity of an absorption threshold, the idler photon generates a set of virtual intermediate states involving a core hole and a corresponding electron excited in a virtual state which can be described by an effective dielectric function ϵ experienced by the valence electrons. Therefore, the effective coupling constant can be modified through the dielectric response if the idler photon

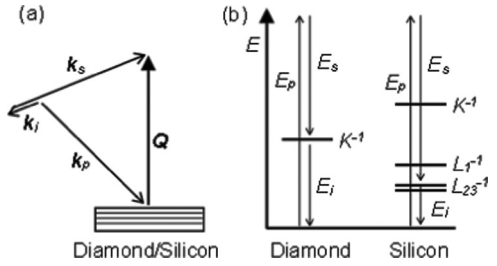

FIG. 1. Schematics explaining the x-ray PDC: (a) momentum conservation law, (b) energy conservation laws in diamond and silicon. The quantities $(E_s,\mathbf{k}_s)$, $(E_i,\mathbf{k}_i)$, and $(E_p,\mathbf{k}_p)$ are the energy momenta of the signal, idler, and pump photons, respectively.

energy is tuned near the binding energy of a core electron level in certain materials.

In general, the dimensionless interaction of quantum electrodynamics (QED) is not constant but varies with the energy scales. In fact, the vacuum of QED can be considered as some kind of polarizable medium where virtual pairs of fermions and antifermions screen the electric charge. For instance, in the standard model of particle physics, the coupling varies because of the crossing of particle production thresholds as illustrated by Jegerlehner [20]. Similarly, in materials, such as FeTe or $TiSe_2$ [16], photons with energies at the proximity of the L_3-absorption threshold generate a set of virtual intermediate states involving a $2p$ core hole and a corresponding electron excited in a $3d$ state, which can be described by an effective dielectric function experienced by the valence electrons. Therefore, we can reduce the dimensionless interaction strength g in a material by introducing photons with energies just below the threshold of x-ray edges, thereby increasing dielectric screening. Consequently, the x-ray scattering cross section σ can be significantly enhanced due to an increased background polarizability. The connection between the effective coupling g and the length scale $\ell = \sqrt{\sigma}$ can be described by a renormalization-group equation,

$$\beta(g) = \frac{dg}{d\ \ln(\ell)}, \tag{2}$$

where the function $\beta(g) = -3g^2$ was derived from a thermodynamic argument [21] involving a pressure needed to set the scale of ℓ for a given coupling g. The solution of Eq. (2) implies that the x-ray scattering cross section σ is renormalized by the factor,

$$\eta = \exp\left[\frac{2}{3\alpha}(\epsilon_1/\epsilon_0 - 1)\right], \tag{3}$$

where ϵ_0 is the dielectric constant in vacuum, α is the fine-structure constant (i.e., the effective coupling g when $\epsilon = \epsilon_0$), and ϵ_1 is the real part of an effective dielectric function ϵ. Near absorption edges, there are anomalous dispersions that allow x-ray PDC to be enhanced within a narrow energy range since ϵ_1/ϵ_0 can be larger from unity in this energy domain. As already mentioned above, the Compton scattering mixes with the PDC, and both processes experience the same renormalization factor η because they involve the same valence electrons embedded in the effective medium described by ϵ. Zambianchi [22] noticed that $|\chi^{(2)}|^2$ is proportional to the cross section. Hence, the renormalization of the cross section also yields a renormalization for $|\chi^{(2)}|^2$ given by

$$|\chi^{(2)}|^2 = \eta\left|\chi^{(2)}_{NR}\right|^2, \tag{4}$$

where $|\chi^{(2)}_{NR}|^2$ represents the nonresonant part of the nonlinear susceptibility. The real part of the dielectric function ϵ_1/ϵ_0 contained in the exponent of η depends on the atomic scattering factor f_1 through the equation,

$$\frac{\epsilon_1}{\epsilon_0} = 1 - \frac{4\pi r_0 \rho}{k_i^2} f_1, \tag{5}$$

where k_i is the norm of the idler wave vector, r_0 is the classical electron radius, and ρ is the number of C or Si atoms per unit volume. The factor f_1 can be written using the Kramers-Kronig transform [23] as

$$f_1(E) = Z^* + \frac{2}{\pi}\int_0^\infty \frac{\omega f_2(\omega)}{E^2 - \omega^2} d\omega, \tag{6}$$

where Z^* is the effective atomic charge and f_2 is the imaginary part of the complex scattering factor. Thus, f_1 becomes negative when the number of anomalous electrons near the absorption edge [given by the second term on the right side of Eq. (6)] is greater than the number of electrons. Moreover, both f_1 and ϵ_1 contain the Lorentz oscillator for the core electrons appearing also in the treatment of RIXS and in a fit of $|\chi^{(2)}|$ proposed by Tamasaku *et al.* [14]. Nevertheless, one should notice that in resonant PDC, ϵ_1 depends of the idler energy whereas in RIXS, ϵ_1 is a function of the incident energy of the photons [15].

III. COMPUTATIONAL AND EXPERIMENTAL METHODS

Henke *et al.* [23] have provided a complete tabulation of values for the atomic scattering factor f_1 calculated for all the elements $Z = 1$–92 in the energy range from 50 eV to 30 keV. However, their atomiclike assumption is clearly insufficient in the vicinity of absorption edges because of condensed-matter effects [24]. For this reason, we have calculated the atomic scattering factor from the program FDMNES (standing for finite difference method near-edge structure) [25], which is a first-principles free and open source code. The program directly calculates the complex scattering factor $f = f_1 + if_2$ without using the Kramers-Kronig transform given by Eq. (6). FDMNES is a real-space program, that does not involve Bloch states and Brillouin-zone samplings. Therefore, whether one considers a molecule or a periodic system, FDMNES builds a cluster around the absorbing atom. The cluster's radius is chosen large enough in order to achieve convergence with respect to the accuracy of the calculation of the final states. The program performs density-functional theory (DFT) self-consistent calculations in the ground and the excited states. The excited-state calculation at a given edge involves the presence of the corresponding core hole. The computed wave functions provide the matrix elements for the direct calculation of the complex scattering factors. We have used the default exchange-correlation potential of FDMNES, which is within the local density approximation (LDA). In fact, the gradient correction to LDA does not give a notable difference for C and Si. The core-level energy is adjusted to the

experiment. Many-body corrections have been implemented via a time-dependent DFT (TDDFT) kernel [26] containing the Hartree term (which gives the main effects) and an exchange-correlation LDA term. We will check that the present TDDFT procedure in Si is validated by a very good agreement with reflectivity experiments. The lattice constants used in the present calculations were 3.56 and 5.43 Å for diamond and Si, respectively. For diamond, $\rho = 1.77 \times 10^{23}$ cm^{-3} whereas for Si, $\rho = 0.50 \times 10^{23}$ cm^{-3}. After obtaining the self-consistent electronic structure, f_1 was computed at the C K edge and at the Si L_{23} edge.

To reveal the resonance effect around the absorption edge, we measured $|\chi^{(2)}|$ of silicon near the L_{23} edge in addition to the previous report on the diamond for the K edge [14] with $\boldsymbol{Q} = (2,2,0)$. The experiments were performed at the 27-m undulator beamline BL19LXU at SPring-8 described by Yabasi and co-workers [27]. The pump photon energy was set to 9.67 keV, which is just above the K edge of Zn. A (111) silicon plate with a thickness of 1.0 mm was used as the nonlinear crystal. The nonlinear diffraction was measured with $\boldsymbol{Q} = (1,1,1)$. The scattering plane was taken on the horizontal plane, and the polarization of the pump x rays is also horizontal. The signal photon energies were selected around the silicon L edge by a bent crystal analyzer with a Ge 220 reflection. The photon energy resolution of the analyzer was measured to be 2.7 eV. In order to separate the signal from the pump beam, a 25-μm-thick Zn foil was inserted before the analyzer. The signal photon was monitored by a NaI scintillation counter, whereas the idler photon was deduced by the energy conservation given in Eq. (2).

IV. RESULTS

Figure 2 illustrates the resonant behavior of the nonlinear susceptibility of diamond as a function of the idler energy E_i. The $|\chi^{(2)}_{NR}|$ value fitted with our model is 1.4 × cm^2/StC, where StC means the Gaussian unit of StatCoulomb. This value is consistent with perturbation theory [28]. The corresponding atomic scattering factor f_1 calculated within FDMNES is shown in the top frame of Fig. 2. Near the K-absorption edge, one can notice the negative excursion of f_1 reaching about -11 that allows ϵ_1/ϵ_0 to be larger from unity near the absorption edge. The peak value of the calculated $\epsilon_1/\epsilon_0 - 1$ is 0.033. A similar dielectric function behavior can also be seen in the optical data from the interstellar dust grains of graphite provided by Draine [29]. However, the peak for graphite is smaller than the one for diamond since the higher density of diamond leads $\epsilon_1/\epsilon_0 - 1$ to be larger by approximately the density ratio. In the bottom frame of Fig. 2, the resonant part of the nonlinear susceptibility obtained by Tamasaku *et al.* [14] is compared to the model. The overall agreement between experimental data and η is good below the threshold energy. Some discrepancies above the absorption threshold can be explained by the fact that the present theory neglects some resonant fluorescent effects due to the core electrons [16]. Interestingly, tuning the idler photon energy above 295 eV makes ϵ_1/ϵ_0 be smaller from unity in a certain energy window. Thus, $|\chi^{(2)}|^2$ becomes smaller than $|\chi^{(2)}_{NR}|^2$ in this region.

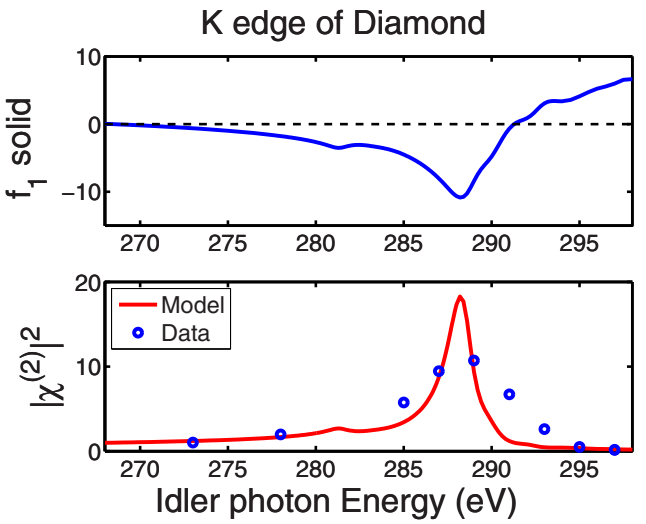

FIG. 2. (Color online) K edge of diamond: In the top frame the solid curve represents the model for f_1 as a function of the idler energy. The label "f_1 solid" emphasizes that the factor f_1 for the solid is different from the one calculated for free atoms. A dashed horizontal line at 0 highlights the f_1 changes in sign. In the bottom frame the black circles and the solid curve are the $|\chi^{(2)}|^2$ in units of $|\chi^{(2)}_{NR}|^2$ and the model for the renormalization factor η, respectively, plotted against the idler energy. The experimental data are reproduced from the experiment by Tamasaku *et al.* [14].

The measured Si rocking curves corresponding to the 111 nonlinear diffraction are shown in Fig. 3. The horizontal axis indicates the deviation angle $\Delta\theta$ from the phase-matching condition at each E_i. When E_i approaches the L_{23} threshold from below the line shape is asymmetric whereas when E_i is well above threshold a dip characterizes the spectrum. The data have been fitted with the Fano formula by Tamasaku *et al.* [14] to extract the ratio $|\chi^{(2)}/\chi^{(2)}_{NR}|^2$ shown in the bottom of Fig. 4. The top of Fig. 4 shows that the FDMNES result for f_1 near the L_{23} edge predicts an amplitude of about -4 after an energy of $E_i = 100$ eV. This result is in good agreement with x-ray reflectivity measurements by Tripathi *et al.* [30] and validates the TDDFT kernel used in FDMNES. In fact, the peak value of the experimental $\epsilon_1/\epsilon_0 - 1$ is 0.024 whereas our calculated value gives 0.025. Clearly, the calculated negative excursion of f_1 leads to good overall agreement with the experimental ratio $|\chi^{(2)}/\chi^{(2)}_{NR}|^2$. Thus, the resonant fluorescent effects neglected by the theory seem to be small at the L_{23} edge of Si. We did not measure the pump intensity in the case of Si, therefore it was not possible to obtain the nonlinear susceptibility in units of cm^2/StC.

Interestingly, the enhancement of $|\chi^{(2)}|$ is not observed at the Si L_1-absorption edge around 150 eV since f_1 does not present any negative excursion in the L_1-edge energy region [24]. Therefore, the sign change in f_1 is a crucial condition for the resonant enhancement of $|\chi^{(2)}|^2$ at a given absorption edge.

V. CONCLUSIONS

We have refuted the claim that the major effect of resonance is a decrease in the strength of PDC. Moreover, we have

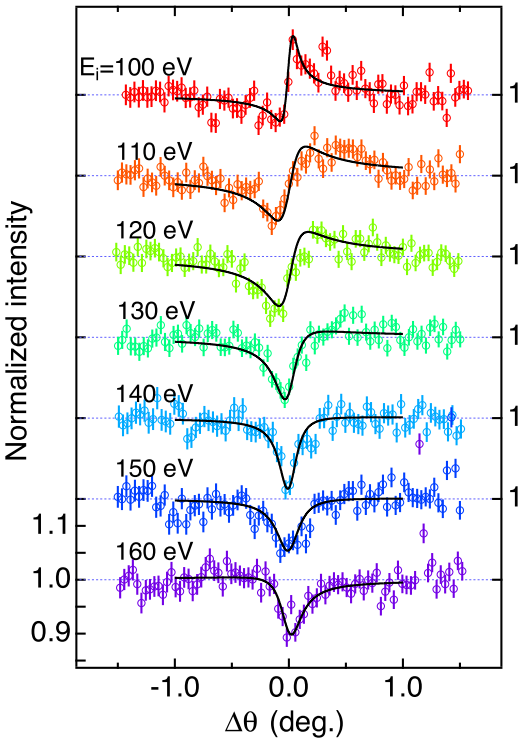

FIG. 3. (Color online) Rocking curves of the 111 nonlinear diffraction of a Si crystal. Circles with error bars represent the measurements, and full lines are fits to the data with the Fano formula used by Tamasaku *et al.* [14].

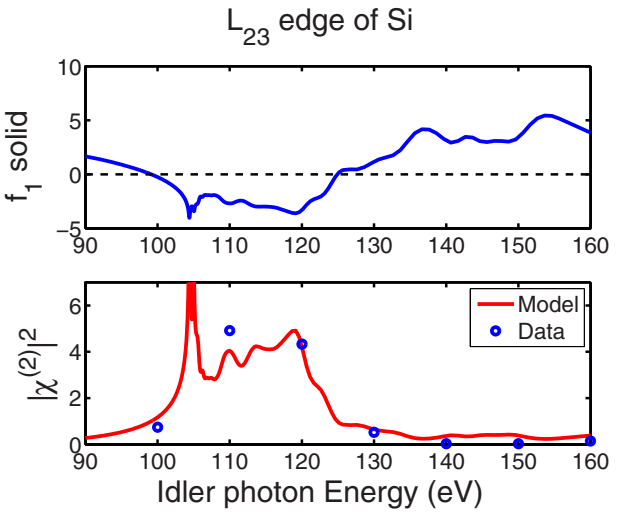

FIG. 4. (Color online) Same as Fig. 2 for the Si L_{23} edge.

explained the factor determining the renormalization of the nonlinear susceptibility $\chi^{(2)}$ at some absorption edges. In our model, the square of the nonlinear susceptibility $|\chi^{(2)}|^2$ has been connected to an effective scattering cross section, whose resonant enhancement is a function of the scattering factor f_1, which is strongly modulated when the idler energy is varied across resonant absorption edges. An important prediction of our scheme is that the resonant enhancement of $|\chi^{(2)}|^2$ for the carbon K edge and the Si L_{23} edge occurs only when f_1 becomes negative otherwise a deenhancement is obtained. This condition for f_1 explains why the resonant enhancement is not observed at the L_1 edge of Si. Our first-principles calculations of f_1 based on FDMNES are able to faithfully reproduce the dispersion at the edges needed for the reliability of the model since they account for bonding and condensed-matter effects. Finally, a related cross-sectional enhancement effect has also been observed in RIXS experiments [16]. Therefore, very accurate RIXS and PDC experiments by XFELs [31] can lead to more fundamental theoretical insight.

ACKNOWLEDGMENTS

We are grateful to G. Volovik for useful discussions on the running coupling constants. This work was supported by the U.S. Department of Energy (DOE), Office of Science, Basic Energy Sciences Grant No. DE-FG02-07ER46352 (core research) and benefited from Northeastern University's Advanced Scientific Computation Center (ASCC), the NERSC supercomputing center through DOE Grant No. DE-AC02-05CH11231, and support (applications to layered materials) from the DOE EFRC: Center for the Computational Design of Functional Layered Materials (CCDM) under Grant No. DE-SC0012575.

[1] R. Bonifacio, C. Pellegrini, and L. M. Narducci, Collective instabilities and high-gain regime in a free electron laser, Opt. Commun. **50**, 373 (1984).

[2] P. Emma *et al.*, First lasing and operation of an ångstrom-wavelength free-electron laser, Nat. Photonics **4**, 641 (2010).

[3] T. Ishikawa *et al.*, A compact X-ray free-electron laser emitting in the sub-ångström region, Nat. Photonics **6**, 540 (2012).

[4] B. W. Adams, in *Nonlinear Optics, Quantum Optics and Ultrafast Phenomena with X-Rays: Physics with X-Ray Free-Electron Lasers*, edited by B. W. Adams (Kluwer Academic, New York, 2003), p. 109.

[5] I. Freund and B. F. Levine, Parametric Conversion of X Rays, Phys. Rev. Lett. **23**, 854 (1969).

[6] P. M. Eisenberger and S. L. McCall, Mixing of X-Ray and Optical Photons, Phys. Rev. A **3**, 1145 (1971).

[7] P. M. Eisenberger and S. L. McCall, X-Ray Parametric Conversion, Phys. Rev. Lett. **26**, 684 (1971).

[8] H. Danino and I. Freund, Parametric Down Conversion of X Rays into the Extreme Ultraviolet, Phys. Rev. Lett. **46**, 1127 (1981).

[9] K. Tamasaku, Kei Sawada, E. Nishibori, and T. Ishikawa, Visualizing the local optical response to extreme-ultraviolet radiation with a resolution of λ/380, Nat. Phys. **7**, 705 (2011).

[10] S. Shwartz, R. N. Coffee, J. M. Feldkamp, Y. Feng, J. B. Hastings, G. Y. Yin, and S. E. Harris, X-Ray Parametric Down-Conversion in the Langevin Regime, Phys. Rev. Lett. **109**, 013602 (2012).

[11] K. Tamasaku and T. Ishikawa, Interference between Compton Scattering and X-Ray Parametric Down-Conversion, Phys. Rev. Lett. **98**, 244801 (2007).

[12] U. Fano, Effects of Configuration Interaction on Intensities and Phase Shifts, Phys. Rev. **124**, 1866 (1961).

[13] A. Vittorini-Orgeas and A. Bianconi, From Majorana Theory of Atomic Autoionization to Feshbach Resonances in High Temperature Superconductors, J. Supercond. Novel Magn. **22**, 215 (2009).

[14] K. Tamasaku, K. Sawada, and T. Ishikawa, Determining X-Ray Nonlinear Susceptibility of Diamond by the Optical Fano Effect, Phys. Rev. Lett. **103**, 254801 (2009).

[15] I. Freund and B. F. Levine, Resonant dispersion of the nonlinear atomic scattering factor, Opt. Commun. **3**, 101 (1971).

[16] B. Barbiellini, J. N. Hancock, C. Monney, Y. Joly, G. Ghiringhelli, L. Braicovich, and T. Schmitt, Inelastic x-ray scattering from valence electrons near absorption edges of FeTe and $TiSe_2$, Phys. Rev. B **89**, 235138 (2014).

[17] L. Landau, in *Niels Bohr and the Development of Physics*, edited by W. Pauli (McGraw-Hill, New York, 1955), p. 52.

[18] N. N. Bogoliubov and D. V. Shirkov, *Quantum Fields* (Benjamin/Cummings, Reading, MA, 1983).

[19] G. E. Volovik, *The Universe in a Helium Droplet* (Oxford University Press, New York, 2008).

[20] F. Jegerlehner, The running fine structure constant $\alpha(E)$ via the Adler function, Nucl. Phys. B **181–182**, 135 (2008).

[21] B. Barbiellini and P. Nicolini, Enhancement of Compton scattering by an effective coupling constant, Phys. Rev. A **84**, 022509 (2011).

[22] P. Zambianchi, in *Nonlinear Optics, Quantum Optics and Ultrafast Phenomena with X-Rays: Physics with X-Ray Free-Electron Lasers*, edited by B. W. Adams (Kluwer Academic, New York, 2003), p. 287.

[23] B. L. Henke, E. M. Gullikson, and J. C. Davis, *X-Ray Interactions: Photoabsorption, Scattering, Transmission, and Reflection at E = 50-30,000 eV, Z = 1-92*, At. Data Nucl. Data Tables **54**, 181 (1993).

[24] M. Nayak and G. S. Lodha, Optical Response Near the Soft X-Ray Absorption Edges and Structural Studies of Low Optical Contrast System Using Soft X-Ray Resonant Reflectivity, J. At., Mol., Opt. Phys. **2011**, 649153 (2011).

[25] O. Bunau and Y. Joly, Self-consistent aspects of x-ray absorption calculations, J. Phys.: Condens. Matter **21**, 345501 (2009).

[26] O. Bunau and Y. Joly, Time-dependent density functional theory applied to x-ray absorption spectroscopy, Phys. Rev. B **85**, 155121 (2012).

[27] M. Yabashi, T. Mochizuki, H. Yamazaki, S. Goto, H. Ohashi, K. Takeshita, T. Ohata, T. Matsushita, K. Tamasaku, Y. Tanaka, and T. Ishikawa, Design of a beamline for the SPring-8 long undulator source 1, Nucl. Instrum. Methods Phys. Res., Sect. A **467–468**, 678 (2001).

[28] An order-of-magnitude estimate obtained from perturbation theory gives $|\chi^{(2)}_{NR}| = \alpha^2 e r_0 \rho/(k_p k_s k_i^2) = 1.2 \times 10^{-16}$ cm^2/StC.

[29] B. T. Draine, Scattering by Interstellar Dust Grains. II. X-Rays, Astrophys. J. **598**, 1026 (2003); http://www.astro.princeton.edu/∼draine/dust/dust.diel.html

[30] P. Tripathi, G. S. Lodha, M. H. Modi, A. K. Sinha, K. J. S. Sawhney, and R. V. Nandedkar, Optical constants of silicon and silicon dioxide using soft X-ray reflectance measurements, Opt. Commun. **211**, 215 (2002).

[31] Near-edge excitation processes may be hindered by the high-intensity regime of XFEL spectroscopy where multiple ionizations of matter can occur during the XFEL impulse. Therefore, the experimental results should be also validated using the synchrotron radiation regime from storage ring sources.